Energy & Environmental Science

Dynamic Article Links

Cite this: *Energy Environ. Sci.*, 2012, **5**, 9085

www.rsc.org/ees

PAPER

Hollow core–shell nanostructure supercapacitor electrodes: gap matters†

Cao Guan,[ac] Xinhui Xia,[a] Nan Meng,[a] Zhiyuan Zeng,[b] Xiehong Cao,[b] Cesare Soci,[a] Hua Zhang[b] and Hong Jin Fan*[ac]

Received 11th July 2012, Accepted 14th August 2012
DOI: 10.1039/c2ee22815g

Hollow core–shell nanorods with a nanogap are designed and constructed with the assistance of atomic layer deposition (ALD) for energy storage applications. As a demonstration, CoO nanorods and NiO nanowalls are enclosed by a TiO_2 nanotube shell, forming the "wire in tube" and "wall in box" structures, respectively. A thin sacrificial layer of Al_2O_3 is deposited by ALD and removed eventually, forming a nanogap between the CoO core (or the NiO nanowall) and the TiO_2 shell. When they are tested as supercapacitor electrodes, an evident difference between the solid core–shell nanostructure and hollow ones can be found; for example, the hollow structure shows ~2 to 4 times the capacitance compared to the solid wires. The electrochemical properties are also superior compared to the bare nanorods without the nanotube shell. The enhancement is ascribed to the conformal hollow design which provides enlarged specific surface areas and a shorter ion transport path. It is prospected that such a positive nanogap effect may also exist in other electrochemical cell electrodes such as lithium ion batteries and fuel cells.

Introduction

With the fossil-fuel crisis and the ever-increasing demand for high-performance portable electronic devices, supercapacitor electrode materials with high specific capacitance, good rate capability and long cycling stability are needed.[1–4] However, the energy density of existing carbon-based supercapacitors is limited, generally to an order of magnitude lower than that of batteries. Transition metal oxides are promising electrode materials of higher energy density as they can store more charges with pseudoreactions while carbon-based materials only store charges electrostatically at their surfaces. However, metal oxides also have problems. In a nutshell, they usually show limited kinetics during the redox reaction with ions as a result of their low electrical conductivity and low surface area compared to carbon.[5–8]

In the research on metal-oxide nanostructured electrodes, several strategies are utilized to construct high-performance supercapacitors. The first is a high specific surface area, that is usually manifested by a porous/hollow feature.[9–20] The large porosity provides easier electrolyte penetration and the hollow center increases the surface-to-bulk ratio thus increasing the contact area between the active material and the electrolyte, leading to more efficient ion transport. Furthermore, improved rate capability and cycling performance can also be achieved

[a]*Division of Physics and Applied Physics, School of Physical and Mathematical Sciences, Nanyang Technological University, 21 Nanyang Link, 637371 Singapore. E-mail: fanhj@ntu.edu.sg*
[b]*School of Materials Science and Engineering, Nanyang Technological University, 639798 Singapore*
[c]*Energy Research Institute@NTU (ERIAN), 50 Nanyang Drive, 637553 Singapore*

† Electronic supplementary information (ESI) available. See DOI: 10.1039/c2ee22815g

Broader context

Hybrid core–shell nanostructures have become a hot research topic in recent years for high-performance supercapacitors. With two functional materials constructed in a programmed way, possible synergetic efforts and better electrochemical properties can be obtained. Porous and hollow structures are also favoured for supercapacitor electrodes as they can provide a large surface area and better rate properties. In this paper, we provide an effective way for the fabrication of hollow core–shell nanostructures with a gap between the core and shell material, with the assistance of atomic layer deposition (ALD). Using CoO–TiO_2 nanorods and nanowalls as examples, we demonstrate that the hollow core–shell structure shows evidently better performance in the supercapacitor test than the solid core–shell ones and bare CoO core. It is anticipated that such hollow core–shell structures have also enhanced performance in other electrochemical devices including Li-ion batteries.

because these void spaces could effectively buffer the strain generated during the fast charge–discharge process.

The second way is direct growth of nanomaterials of metal oxides on current collectors.[21–23] This method ensures good mechanical adhesion and electric connection of the active material to the current collector. Also dead mass could be avoided as the polymer binders and conductive addictives are not used.

Another strategy is to hybridize metal oxides with carbon, conductive polymer and other metal oxides into core–shell structures. This has been proven to be an effective way to combine the merits of the individual components.[24–27] For example, nanostructured MnO_2@NiO,[28] Zn_2SnO_4@MnO_2[24] and CNT@MnO_2[29] have been successfully fabricated and their improved electrochemical performances have been demonstrated when used as supercapacitor electrodes.

Based on the above considerations, we intend to combine all these strategies into one structure by a unique rational design. Herein we report a novel type of "wire in tube" electrode nanomaterial which fulfils nearly all the above favorable requirements. ALD is employed for surface coating of a sacrificial layer of Al_2O_3 and an outer TiO_2 nanotube shell. ALD has been demonstrated as a useful tool technique for surface engineering of electrode materials.[30–35] The obtained "wire in tube" structure has the three major merits: (1) a highly porous 1D core material (CoO nanorod in this case) which is directly grown on metal foams; (2) a thin and uniform nanotube shell (TiO_2 in this case, but could be also other materials when the respective ALD precursors are used) providing a stabilization protection;[36] and (3) a nanogap between the core and the nanotube shell could serve as an "ion reservoir". As a result of this design, compared to the bare nanorod and the solid core–shell wires without gap, the "wire in tube" electrode has larger surface area for electrochemical reaction, faster ion transportation and improved cyclic retention owing to the very stable TiO_2 shell that protects the core. Furthermore, it is possible that the tube shell can also contribute EDLC or pseudocapacitance. Such a unique core–shell "wire in tube" nanoarchitecture could be generalized to many other energy applications by hybridizing with different functionalized shell materials. Our data also verify the usefulness of ALD in nanofabrication and surface engineering of nanoscale electrode materials.

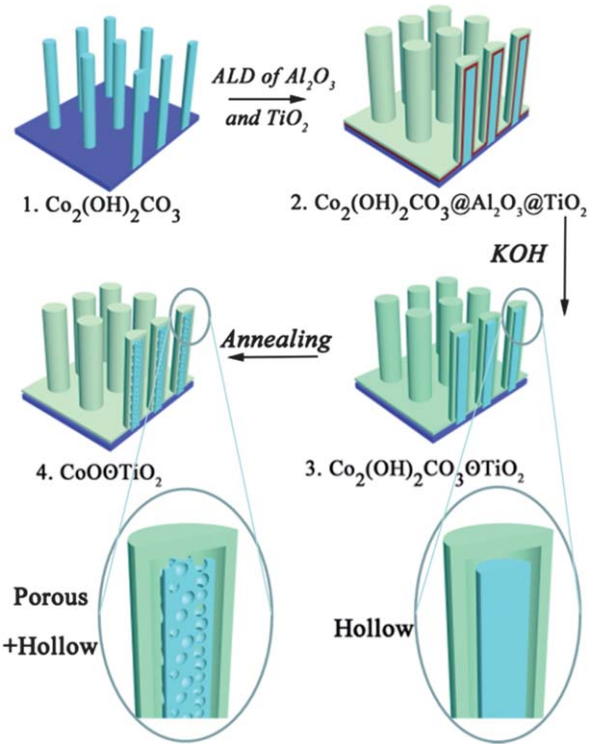

Fig. 1 Illustration of the fabrication process of the "wire in tube" structure of CoO⊙TiO_2.

Experimental details

Material synthesis

The 3D hybrid electrode material was prepared by a three-step process, as illustrated in Fig. 1. (1) The CoO precursor was synthesized on nickel foam by a hydrothermal process. For this, 2 mmol $Co(NO_3)_2 \cdot 6H_2O$, 10 mmol urea and 4 mmol NH_4F were dissolved in 50 ml deionized water, then the obtained homogeneous solution was transferred into a Teflon-lined stainless steel autoclave with a piece of clean nickel foam ($20 \times 50 \times 0.1$ mm^3, with upper side protected by uniform coating of polytetrafluoroethylene tape) immersed into the reaction solution at 120 °C for 8 h growth. (2) The nickel foam with the as-grown CoO nanostructure precursor was coated with Al_2O_3 followed by TiO_2 by ALD of different cycles using a Beneq system (TFS 200) at 120 °C. Trimethylaluminum ($Al(CH_3)_3$), $TiCl_4$ and water were used as the aluminium, titanium and oxygen source, respectively. During deposition, the reaction chamber was maintained at 1.0 mbar with a steady N_2 steam at 200 SCCM (cubic centimeter per minute). Each ALD cycle consisted of a 300 ms precursor pulse and 1 s purging time with N_2. (3) The substrates were immersed in a 0.1 M KOH solution in order to dissolve the Al_2O_3 sandwich layer. After that, the samples were annealed in Ar at 350 °C for 2 h. In the following, we use "CoO⊙TiO_2" to denote the hollow core–shell structure, and "CoO@TiO_2" for the solid core–shell structure.

A similar method was used for the preparation of NiO nanowall in the TiO_2 nanobox structure. The NiO nanowall precursor was prepared by chemical bath deposition with a solution of 80 ml of 1 M nickel sulfate, 60 ml of 0.25 M potassium persulfate and 20 ml of aqueous ammonia (25–28%) in a 150 ml Pyrex beaker at room temperature reacting for 10 min.

Characterization

In order to show clearly the nanogap, before electron microscopy characterization, the top layer of TiO_2 was etched by a reactive ion etching process[30] for 35 s in a PECVD system (Plasmatherm 790 model). A mixture gas of CF_4–O_2 (55 sccm + 5 sccm) was employed with a RF power of 175 W and chamber pressure of 55 mTorr. Samples were characterized by a scanning electron microscope (SEM, JSM-6700F, 10.0 kV) and a transmission electron microscope (TEM, JEM-2010FEF, 200 kV) equipped with an energy dispersive X-ray spectrometer (EDS). The mass of electrode materials was measured on an AX/MX/UMX Balance (METTLER TOLEDO, maximum = 5.1 g; delta = 0.001 mg). Nitrogen adsorption–desorption isotherms were measured on a

Micromeritics TriStar 3000 porosimeter (mesoporous characterization) and a Micromeritics ASAP 2020 (microporous characterization) at 77 K. All samples were outgassed at 100 °C for 6 h under vacuum before measurements were recorded. The specific surface areas were calculated using the Brunauer–Emmett–Teller (BET) method.

Electrochemical measurement

Electrochemical measurements using a workstation (CHI 760D) were carried out in a three-electrode electrochemical cell at room temperature using 2 M KOH as electrolyte. The nickel foam supported nanostructure (~2 cm^2 area; CoO mass: ~3.6 mg cm^{-2}; CoO⊙TiO_2 mass: ~4.5 mg cm^{-2}, NiO mass: ~0.5 mg cm^{-2}, and NiO⊙TiO_2 mass: ~0.7 mg cm^{-2}) acted directly as the working electrode. A Pt plate and Hg/HgO were used as the counter electrode and the reference electrode, respectively. All potentials were referred to the reference electrode. The weight in specific capacitance (F g^{-1}) and current rate (A g^{-1}) was calculated based on the whole mass of the active materials (CoO, NiO and TiO_2), and the small contribution from the Ni foam was subtracted. The specific capacitance is calculated by $C = It/m\Delta V$ and the areal capacitance is calculated by: $C_a = It/(\Delta VS)$, where I is the discharge current, t is the discharge time, m is the mass of the active materials, ΔV is the voltage drop upon discharging, and S is the geometrical area of the electrode. Electrochemical impedance spectroscopy (EIS) measurements were carried out by applying an AC voltage with 1 mV amplitude in a frequency range from 0.1 Hz to 100 kHz at open circuit potential.

Results and discussion

Nanostructure of wire-in-tube design

Morphologies of the core–shell hollow nanorods were examined using SEM. The bare CoO nanorods cover uniformly on the substrate surface (Fig. 2a). The enlarged image (inset of Fig. 2a) shows that the nanorods are highly porous. The large-scale SEM image of the sample can also be seen in the ESI (Fig. S1a†). The uniform growth of metal oxides by solution methods on nickel foam can be found in many literatures.[37–41] After ALD coating of an Al_2O_3–TiO_2 bilayer (ALD cycles of 80/165 were used for all the following experiments), the nanowires become thicker and smoother (Fig. S1b and c†). After removing the Al_2O_3 layer by KOH and annealing, the structure does not collapse (Fig. S1d†) but its hollow nature can be hardly inspected based on SEM images. In order to disclose the hollow structure, the thin top layer was removed by ion milling. One can see clearly from Fig. 2b and c the hollow core–shell structure, in which the porous CoO nanorod is enclosed by a thin tube layer with a small gap.

The hollow structure can be revealed more clearly by TEM. The porous CoO nanorods are assembled by numerous interconnected nanoparticles (Fig. 2d).[42] For CoO⊙TiO_2, the typical TEM image in Fig. 2e shows clearly that the porous CoO is enclosed by a thin and continuous layer of TiO_2 with a nanogap in between. Both the tube layer of TiO_2 and the gap layer after removal of the ALD Al_2O_3 sandwich layer are uniform in thickness, owing to the conformity of ALD.[43] Direct coating of ALD TiO_2 on the CoO nanorods resulted in a solid CoO@TiO_2 core–shell structure without nanogap (see TEM images in the ESI†).

The atomic structure of the CoO⊙TiO_2 nanorods was investigated by high-resolution TEM (HRTEM). From images recorded from three different areas marked in Fig. 3a, the crystalline property of the structure can be revealed. The core CoO has a cubic lattice distance of 0.21 nm corresponding to the (200) d-spacing. The lattice fringes of the outer shell show a distance of about 0.35 nm, which matches the (101) planes of anatase TiO_2. These values accord well with the previously reported ones for hydrothermal grown CoO nanorods[44] and the TiO_2 tubes by ALD.[45] It is noted that at a relatively low deposition temperature (120 °C in this case), there are no solid state reactions between the three materials towards the alloy formation.[45,46]

The hollow core–shell structure has a higher surface area as confirmed by the BET measurement. The surface area of the bare CoO nanorods on nickel foam is 7.28 m^2 g^{-1}. After

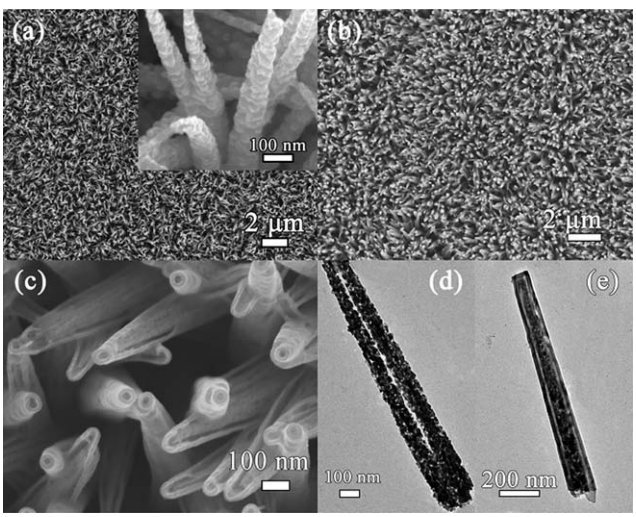

Fig. 2 SEM images of (a) CoO nanorod and (b and c) "wire in tube" structure of CoO⊙TiO_2. TEM images of (d) two CoO nanorods and (e) "wire in tube" structure of CoO⊙TiO_2.

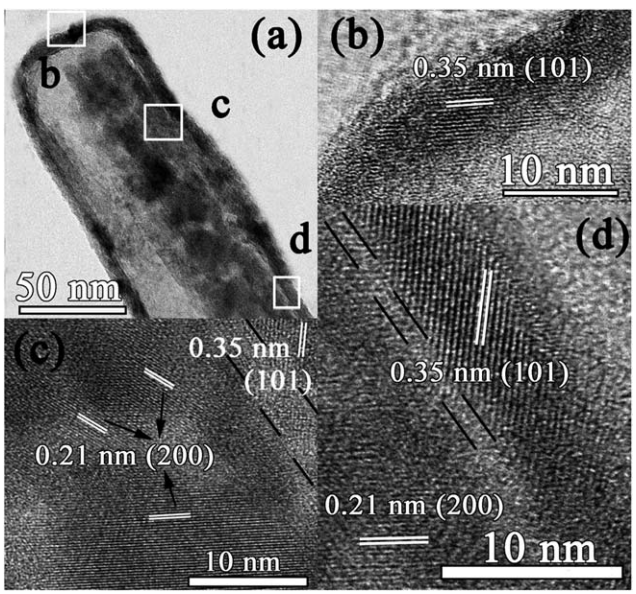

Fig. 3 HRTEM characterization of a typical CoO⊙TiO_2 "wire in tube" structure.

transformation to the hollow core–shell structure, it increases to 11.63 m^2 g^{-1}. In contrast, direct coating of TiO_2 on the porous CoO reduced the surface area to 5.63 m^2 g^{-1}. Therefore the CoO⊙TiO_2 has a larger surface in contact with electrolyte, which would be beneficial to its electrochemical performance.

Electrochemical property of the wire-in-tube electrode

The electrochemical properties of the "wire in tube" structure were investigated in detail as follows. Fig. S2a† shows the CV curves of the three structures: CoO, CoO@TiO_2 and CoO⊙TiO_2. The CoO has two pairs of redox peaks in the CV curve: $CoO + OH^- \leftrightarrow CoOOH + e^-$ and $CoOOH + OH^- \leftrightarrow CoO_2 + H_2O + e^-$, which are consistent with the previous report.[47] After direct coating of TiO_2, the enclosed area of the CV curve is decreased, which means less active materials are reacting with the electrolyte. For the hollow core–shell CoO⊙TiO_2, the enclosed area of its CV loop is larger than the bare CoO nanorod sample, which indicates an increase in areal capacitance. In addition, the current densities of the CoO⊙TiO_2 hollow core–shell wires are higher than those of other counterparts, implying their better electrochemical reactivity. Although TiO_2 has a low pseudocapacitance,[48–50] the structure of CoO⊙TiO_2 still shows an areal capacitance of 52.4% higher than the bare CoO sample, and the specific capacitance is also increased from 518.9 F g^{-1} to 633.3 F g^{-1}.

Similar results can also be obtained from charge–discharge tests (Fig. 4a). At the same areal current density of 10 mA cm^{-2}, the solid core–shell CoO@TiO_2 has an areal specific capacitance of only 0.745 F cm^{-2}, which is only 39.8% of that of bare CoO (1.87 F cm^{-2}). However, the hollow "wire in tube" structure has a specific capacitance of 2.85 F cm^{-2}, 3.83 times that of the CoO@TiO_2. Based on the mass of the three electrodes, the specific capacitance of CoO, CoO@TiO_2 and CoO⊙TiO_2 is 518.9, 187.7 and 633.3 F g^{-1}, respectively. The charge–discharge curves of the CoO and CoO⊙TiO_2 are shown in Fig. S2b and c.†

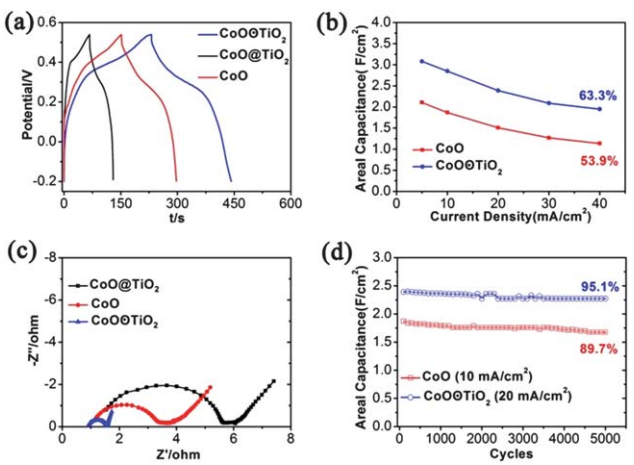

Fig. 4 (a) Charge–discharge curve of the three structures (CoO, CoO@TiO_2 and CoO⊙TiO_2) at the same current density of 10 mA cm^{-2}. (b) Rate capability of the CoO and CoO⊙TiO_2. The percentage numbers denote the capacitance retention when the current is increased from 5 to 40 mA cm^{-2}. (c) Electrochemical impedance spectroscopy of the three structures. (d) Cycling stability of the CoO and CoO⊙TiO_2. The percentage numbers denote the capacitance retention after 5000 cycles of charge–discharge.

The rate capability of the CoO⊙TiO_2 is also improved (see Fig. 4b). When the current density increased from 5 to 40 mA cm^{-2}, the CoO⊙TiO_2 has a 63.3% capacitance retention compared to 53.9% of CoO, which means the structure of CoO⊙TiO_2 can better maintain the electrolyte contact for reaction even in fast charge–discharge processes.

Electrochemical impedance spectroscopy (EIS) is a useful method to evaluate the transport property of an electrochemical system. Results of EIS on the three materials are shown in Fig. 4c. In the high frequency region, the semicircle corresponds to the charge-transfer resistance at the electrode/electrolyte interface. The structure of CoO⊙TiO_2 shows the smallest radius, which means it is most suitable for charge transport with the electrolyte. The CoO@TiO_2 sample has the largest charge-transfer resistance, which is within expectation since the solid TiO_2 shell retards the charge transfer. In the low frequency regime, CoO⊙TiO_2 also displays a more ideal straight line along the imaginary axis, which demonstrates its low diffusion resistance. The low diffusion and electron-transfer resistances of the CoO⊙TiO_2 revealed by EIS measurement are in good accordance with its above-mentioned electrochemical performance.

Finally, as one of the key issues for supercapacitor electrode materials, the cycling stability has been tested for the two electrodes (Fig. 4d). The CoO itself has a very good stability (89.7% capacitance retention after 5000 cycles at 10 mA cm^{-2}), yet the CoO⊙TiO_2 shows a slightly better capacitance retention (95.1% after 5000 cycles) at a higher current density (20 mA cm^{-2}).

We now discuss the mechanisms of the enhancement in pseudocapacitive performance of the "wire in tube" structure. Three possible factors might play the role. First, the nanogap effectively creates a spatial confinement to the electrolyte between the CoO core and the ALD shell. Within this gap, a close contact between CoO and electrolyte is ensured enabling a rapid ion transport. The gap serves as an "ion reservoir" preserving the relatively stable supply of OH^- even at high current densities. This may explain the improved rate capability of CoO⊙TiO_2, which is also supported by the fact that the capacitance increase is more evident at higher current densities (71.7% improvement with respect to the CoO at a high current density of 40 mA cm^{-2}, see Fig. 4b).

As for the solid core–shell wires, the dense ALD TiO_2 layer creates a diffusion barrier (but not block) for the OH^- ions to reach the CoO core, as demonstrated by the EIS result. This explains why the CoO@TiO_2 sample has the largest charge-transfer resistance.

Second, the specific surface area is increased due to the thin nanotube wall. In general, a conformal coating of shell material can increase the surface area several times.[51] If the TiO_2 nanotube shell is connected to the CoO core at any point, it effectively contributes to pseudocapacitance in a similar way to the AC-based EDLCs,[50] and the physical charge on the wall of TiO_2 shell can be transported eventually to the current collector.

Third, TiO_2 is a quite stable electrochemical system (note the recent increasing interests in nano TiO_2 in Li-ion batteries[52,53]). The thin and conformal ALD TiO_2 shell protects the core materials from structural deterioration during prolonged charge–discharge cycles. This may explain the improved capacity retention of the hollow core–shell CoO⊙TiO_2 nanorods compared to the bare CoO nanorods (Fig. 4d).

By changing the ALD cycles of Al_2O_3 and TiO_2, several "wire in tube" structures with different thicknesses of hollow layer and tube layer can be obtained (typical TEM images can be seen in Fig. S3a–f†). All the "wire in tube" structures show improved performance in charge–discharge tests than the CoO nanorods alone, and the structure with 20/110 ALD cycles of Al_2O_3–TiO_2 gives the largest areal capacitance (see Fig. S3g†).

Wall-in-box nanostructured electrode

To check the generality of the nanogap design, another hollow core–shell structure of "wall in box" was fabricated and tested. Fig. 5a shows the SEM image of the vertically aligned, interconnected NiO nanowalls. After the similar treatment procedure to the above CoO nanorods (*i.e.*, ALD coatings of Al_2O_3 and TiO_2 followed by removal of Al_2O_3), the NiO nanowalls become thicker (see Fig. 5b). After ion milling, the nanogap can be clearly seen (inset of Fig. 5b). The NiO nanowall in TiO_2 nanobox (denoted by NiO⊙TiO_2) also showed an increased areal capacitance, as illustrated by CV and CD results (in Fig. 5c and d). In addition, the rate capability of NiO⊙TiO_2 has also increased as it shows a 64.3% capacitance retention when the current increased 10 times, compared to 58.4% of the bare NiO nanowall (see Fig. S4a†). The enhanced cycling stability is also achieved as shown in Fig. S4b.† All these improvements are consistent with that of the porous nanorods, and further corroborate the advantage of the hollow core–shell structure design.

It is noteworthy that in this hollow electrode design, the materials for the gap layer and outer shell are not limited to Al_2O_3 and TiO_2, respectively. In particular, the TiO_2 shell could be replaced with carbon, or more electrochemically active oxides such as NiO and Co_3O_4. Better performance is expected if such a pseudocapacitive shell can be also coated by ALD.

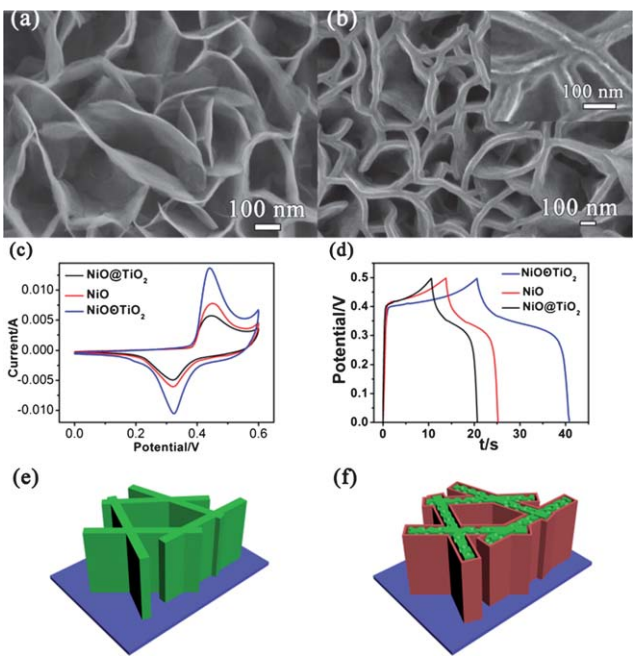

Fig. 5 SEM images of (a) NiO nanowall and (b) "wall in box" structure of NiO⊙TiO_2. (c) CV and (d) charge–discharge curves of the three structures (NiO, NiO@TiO_2 and Ni⊙TiO_2). (e and f) Schematics of the NiO nanowall and NiO⊙TiO_2 wall-in-wall structure.

In conclusion, we have proposed and demonstrated a general concept of the "gapped core–shell nanostructures" for electrochemical energy storage application. With the assistance of ALD, "wire in tube" and "wall in box" structures of CoO–TiO_2 are fabricated and tested. The hollow core–shell electrodes with nanogap show evidently higher areal capacitance than the solid core–shell nanorods without gap, as well as improved rate capability and cycling ability. It is proposed that the nanogap provides an increased reaction area and facilitates the electrolyte contact with the active material. In addition, the outer tube layer also preserves the structural integrity after long-time cycling. Such a hollow core–shell nanostructure represents an effective way to improve the electrochemical performance of metal oxide-based supercapacitors. Further improvement in areal capacitance can be expected by choosing more electrochemically active shell materials (such as NiO) and fine adjustment of the gap thickness.

Acknowledgements

This research is supported by SERC Public Sector Research Funding (grant number 1121202012), Agency for Science, Technology, and Research (A*STAR).

Notes and references

1 C. Liu, F. Li, L.-P. Ma and H.-M. Cheng, *Adv. Mater.*, 2010, **22**, E28–E62.
2 G. Wang, L. Zhang and J. Zhang, *Chem. Soc. Rev.*, 2012, **41**, 797–828.
3 P. Simon and Y. Gogotsi, *Nat. Mater.*, 2008, **7**, 845–854.
4 P. J. Hall, M. Mirzaeian, S. I. Fletcher, F. B. Sillars, A. J. R. Rennie, G. O. Shitta-Bey, G. Wilson, A. Cruden and R. Carter, *Energy Environ. Sci.*, 2010, **3**, 1238–1251.
5 X. Zhao, B. M. Sanchez, P. J. Dobson and P. S. Grant, *Nanoscale*, 2011, **3**, 839–855.
6 Z.-S. Wu, G. Zhou, L.-C. Yin, W. Ren, F. Li and H.-M. Cheng, *Nano Energy*, 2012, **1**, 107–131.
7 W. Deng, X. Ji, Q. Chen and C. E. Banks, *RSC Adv.*, 2011, **1**, 1171–1178.
8 G. Lota, K. Fic and E. Frackowiak, *Energy Environ. Sci.*, 2011, **4**, 1592–1605.
9 X. Lai, J. E. Halpert and D. Wang, *Energy Environ. Sci.*, 2012, **5**, 5604–5618.
10 C.-Y. Cao, W. Guo, Z.-M. Cui, W.-G. Song and W. Cai, *J. Mater. Chem.*, 2011, **21**, 3204–3209.
11 S. Ding, T. Zhu, J. S. Chen, Z. Wang, C. Yuan and X. W. Lou, *J. Mater. Chem.*, 2011, **21**, 6602–6606.
12 Z. Lu, Z. Chang, W. Zhu and X. Sun, *Chem. Commun.*, 2011, **47**, 9651–9653.
13 M. Xu, L. Kong, W. Zhou and H. Li, *J. Phys. Chem. C*, 2007, **111**, 19141–19147.
14 X. Zhang, W. Shi, J. Zhu, W. Zhao, J. Ma, S. Mhaisalkar, T. Maria, Y. Yang, H. Zhang, H. Hng and Q. Yan, *Nano Res.*, 2010, **3**, 643–652.
15 X.-H. Xia, J.-P. Tu, Y.-J. Mai, X.-L. Wang, C.-D. Gu and X.-B. Zhao, *J. Mater. Chem.*, 2011, **21**, 9319–9325.
16 C. Guan, X. Li, Z. Wang, X. Cao, C. Soci, H. Zhang and H. J. Fan, *Adv. Mater.*, 2012, **24**, 4186–4190.
17 J. Zhu, W. Shi, N. Xiao, X. Rui, H. Tan, X. Lu, H. H. Hng, J. Ma and Q. Yan, *ACS Appl. Mater. Interfaces*, 2012, **4**, 2769–2774.
18 Z. Li, X. Lai, H. Wang, D. Mao, C. Xing and D. Wang, *J. Phys. Chem. C*, 2009, **113**, 2792–2797.
19 W. Xia, W. Meng, R. Yu, X. Xing, D. Wang, Y. Chen and M. Takano, *Chem. Lett.*, 2006, 656–657.
20 H. Guan, X. Wang, H. Li, C. Zhi, T. Zhai, Y. Bando and D. Golberg, *Chem. Commun.*, 2012, **48**, 4878–4880.

21 J. Jiang, J. P. Liu, X. T. Huang, Y. Y. Li, R. M. Ding, X. X. Ji, Y. Y. Hu, Q. B. Chi and Z. H. Zhu, *Cryst. Growth Des.*, 2009, **10**, 70–75.
22 J. Zhu, J. Jiang, J. Liu, R. Ding, H. Ding, Y. Feng, G. Wei and X. Huang, *J. Solid State Chem.*, 2011, **184**, 578–583.
23 L. Yang, S. Cheng, Y. Ding, X. Zhu, Z. L. Wang and M. Liu, *Nano Lett.*, 2011, **12**, 321–325.
24 G. Yu, L. Hu, M. Vosgueritchian, H. Wang, X. Xie, J. R. McDonough, X. Cui, Y. Cui and Z. Bao, *Nano Lett.*, 2011, **11**, 2905–2911.
25 L. Bao, J. Zang and X. Li, *Nano Lett.*, 2011, **11**, 1215–1220.
26 H. Wang, H. S. Casalongue, Y. Liang and H. Dai, *J. Am. Chem. Soc.*, 2010, **132**, 7472–7477.
27 X. Cao, Y. Shi, W. Shi, G. Lu, X. Huang, Q. Yan, Q. Zhang and H. Zhang, *Small*, 2011, **7**, 3163–3168.
28 J. Liu, J. Jiang, M. Bosman and H. J. Fan, *J. Mater. Chem.*, 2012, **22**, 2419–2426.
29 S. W. Lee, J. Kim, S. Chen, P. T. Hammond and Y. Shao-Horn, *ACS Nano*, 2010, **4**, 3889–3896.
30 L. K. Tan, M. A. S. Chong and H. Gao, *J. Phys. Chem. C*, 2007, **112**, 69–73.
31 I. D. Scott, Y. S. Jung, A. S. Cavanagh, Y. Yan, A. C. Dillon, S. M. George and S.-H. Lee, *Nano Lett.*, 2010, **11**, 414–418.
32 S. Boukhalfa, K. Evanoff and G. Yushin, *Energy Environ. Sci.*, 2012, **5**, 6872–6879.
33 X. Li, X. Meng, J. Liu, D. Geng, Y. Zhang, M. N. Banis, Y. Li, J. Yang, R. Li, X. Sun, M. Cai and M. W. Verbrugge, *Adv. Funct. Mater.*, 2012, **22**, 1647–1654.
34 Y. S. Jung, A. S. Cavanagh, L. A. Riley, S.-H. Kang, A. C. Dillon, M. D. Groner, S. M. George and S.-H. Lee, *Adv. Mater.*, 2010, **22**, 2172–2176.
35 J. W. Elam, D. Routkevitch, P. P. Mardilovich and S. M. George, *Chem. Mater.*, 2003, **15**, 3507–3517.
36 G. Yu, L. Hu, N. Liu, H. Wang, M. Vosgueritchian, Y. Yang, Y. Cui and Z. Bao, *Nano Lett.*, 2011, **11**, 4438–4442.
37 X.-H. Xia, J.-P. Tu, Y.-Q. Zhang, Y.-J. Mai, X.-L. Wang, C.-D. Gu and X.-B. Zhao, *RSC Adv.*, 2012, **2**, 1835–1841.
38 X.-H. Xia, J.-P. Tu, X.-L. Wang, C.-D. Gu and X.-B. Zhao, *Chem. Commun.*, 2011, **47**, 5786–5788.
39 X. Qing, S. Liu, K. Huang, K. Lv, Y. Yang, Z. Lu, D. Fang and X. Liang, *Electrochim. Acta*, 2011, **56**, 4985–4991.
40 Y. Gao, S. Chen, D. Cao, G. Wang and J. Yin, *J. Power Sources*, 2010, **195**, 1757–1760.
41 Q. Yang, Z. Lu, Z. Chang, W. Zhu, J. Sun, J. Liu, X. Sun and X. Duan, *RSC Adv.*, 2012, **2**, 1663–1668.
42 J. Liu, J. Jiang, C. Cheng, H. Li, J. Zhang, H. Gong and H. J. Fan, *Adv. Mater.*, 2011, **23**, 2076–2081.
43 T. R. B. Foong, Y. Shen, X. Hu and A. Sellinger, *Adv. Funct. Mater.*, 2010, **20**, 1390–1396.
44 J. Jiang, J. Liu, R. Ding, X. Ji, Y. Hu, X. Li, A. Hu, F. Wu, Z. Zhu and X. Huang, *J. Phys. Chem. C*, 2009, **114**, 929–932.
45 C. Bae, Y. Yoon, H. Yoo, D. Han, J. Cho, B. H. Lee, M. M. Sung, M. Lee, J. Kim and H. Shin, *Chem. Mater.*, 2009, **21**, 2574–2576.
46 X. Chu, X. Liu, G. Wang and G. Meng, *Mater. Res. Bull.*, 1999, **34**, 1789–1795.
47 C. Guan, J. Liu, C. Cheng, H. Li, X. Li, W. Zhou, H. Zhang and H. J. Fan, *Energy Environ. Sci.*, 2011, **4**, 4496–4499.
48 X. Lu, G. Wang, T. Zhai, M. Yu, J. Gan, Y. Tong and Y. Li, *Nano Lett.*, 2012, **12**, 1690–1696.
49 J. Wang, J. Polleux, J. Lim and B. Dunn, *J. Phys. Chem. C*, 2007, **111**, 14925–14931.
50 M. S. Kim, T.-W. Lee and J. H. Park, *J. Electrochem. Soc.*, 2009, **156**, A584–A588.
51 D. Gu, H. Baumgart, T. M. Abdel-Fattah and G. Namkoong, *ACS Nano*, 2010, **4**, 753–758.
52 Z. Hong, M. Wei, T. Lan, L. Jiang and G. Cao, *Energy Environ. Sci.*, 2012, **5**, 5408–5413.
53 Z. Chen, D. Zhang, X. Wang, X. Jia, F. Wei, H. Li and Y. Lu, *Adv. Mater.*, 2012, **24**, 2030–2036.

